Dynamics of rising bubble inside a viscosity-stratified medium

A. R. Premlata, Manoj Kumar Tripathi, and Kirti Chandra Sahu

Citation: Physics of Fluids **27**, 072105 (2015); doi: 10.1063/1.4927521
View online: http://dx.doi.org/10.1063/1.4927521
View Table of Contents: http://scitation.aip.org/content/aip/journal/pof2/27/7?ver=pdfcov
Published by the AIP Publishing

PHYSICS OF FLUIDS **27**, 072105 (2015)

Dynamics of rising bubble inside a viscosity-stratified medium

A. R. Premlata, Manoj Kumar Tripathi, and Kirti Chandra Sahu[a)]
Department of Chemical Engineering, Indian Institute of Technology Hyderabad, Yeddumailaram 502 205, Telangana, India

(Received 3 February 2015; accepted 17 July 2015; published online 30 July 2015)

The rising bubble dynamics in an unconfined quiescent viscosity-stratified medium has been numerically investigated. This is frequently encountered in industrial as well as natural phenomena. In spite of the large number of studies carried out on bubbles and drops, very few studies have examined the influence of viscosity stratification on bubble rise dynamics. To the best of our knowledge, none of them have isolated the effects of viscosity-stratification alone, even though it is known to influence the dynamics extensively, which is the main objective of the present study. By conducting time-dependent simulations, we present a library of bubble shapes in the Galilei and the Eötvös numbers plane. Our results demonstrate some counter-intuitive phenomena for certain range of parameters due to the presence of viscosity stratification in the surrounding fluid. We found that in a linearly increasing viscosity medium, for certain values of parameters, bubble undergoes large deformation by forming an elongated skirt, while the skirt tends to physically separate the wake region from the rest of the surrounding fluid. This peculiar dynamics is attributed to the migration of less viscous fluid that is carried in the wake of the bubble as it rises, and thereby creating an increasingly larger viscosity contrast between the fluid occupied in the wake region and the surrounding fluid, unlike that observed in a constant viscosity medium. It is also observed that the effect of viscosity stratification is qualitatively different for different regimes of the dimensionless parameters. In future, it will be interesting to investigate this problem in three-dimensions. © *2015 AIP Publishing LLC*. [http://dx.doi.org/10.1063/1.4927521]

I. INTRODUCTION

The dynamics of rising bubble in a quiescent liquid has been of interest for more than a century. In many natural phenomena, such as aerosol transfer from sea, oxygen dissolution in lakes due to rain and electrification of atmosphere by sea bubbles,[1] carbon sequestration,[2] and in industrial applications such as bubble column reactors, the surrounding fluid viscosity may not be constant. The viscosity stratification can occur due to several factors, for instance, due to the presence of gradients in temperature and concentration of some species/solutes. For instance, the viscosity of water or milk is made to increase by almost three orders of magnitude by the addition of only 2% carboxymethylcellulose (CMC)[3] in the ice-cream and lotion industries. Note that the density changes due to such an addition of the species (CMC) are negligible while varying the viscosity by a large amount. The viscosity in the underground crude oil reservoirs may vary up to three orders of magnitude.[4] Also, the viscosity stratification is observed because of the variation in composition of the crude oil with depth. In contrast to this, the density does not change by even an order of magnitude within the reservoir. Carbon-dioxide flooding is a common method used for the recovery of crude oil, which may lead to the formation of bubbles of carbon-dioxide in the crude oil. Also, viscosity of molten silicates and metals can be made to vary across several orders of magnitude[5] by maintaining a temperature difference of a few hundreds of degrees Celsius between the top

a)ksahu@iith.ac.in

and the bottom walls of a domain. However, the gradients of temperature or concentration at the liquid-gas interface can also give rise to surface tension gradients, which in turn induce tangential stresses, known as Marangoni stresses. This forces the fluid to migrate in the vicinity of the interface separating the fluids. Marangoni flows can be of great importance to a large variety of industrial applications and thus have been investigated by several researchers.[6–13]

The bubble dynamics due to the temperature gradient was first studied by Young *et al.*[6] They experimentally investigated rise of small or large air bubbles in a container heated from below. In this study, the resultant dynamics is due to the competition of buoyancy and thermocapillary forces. For small air bubbles, they found that for some imposed temperature gradient, the induced Marangoni stresses acting in the downward direction overcome the buoyancy force, and the bubbles move in the downward direction. However, larger bubbles continue to move in the upward direction. In the later case, buoyancy force is the winner. Since then this problem has been studied experimentally, numerically, and theoretically by several researchers.[6–12] Recently, Tripathi *et al.*[13] studied the dynamics of rising bubble inside a tube wherein temperature along the wall linearly increases in the upward direction. They considered the surrounding fluid to be of "self-rewetting" type, for which surface tension and temperature dependence are non-monotonic. By considering a quadratic dependence of surface tension on temperature, they found that even though this condition is favourable for bubble rise (in case of common fluids, e.g., air, water, and viscous oil), the motion of the bubble can be reversed and then arrested in "self-rewetting" fluids (e.g., high carbon alcohol solutions). Furthermore, they found that under certain conditions, bubble elongated significantly as it rose through the tube. Also, by conducting numerical simulations, Merritt *et al.*[14] studied the effect of buoyancy and thermocapillarity on rising bubble dynamics. In the limit of large Reynolds and Marangoni numbers, Balasubramaniam[15] studied this problem by an asymptotic analysis. They also included the temperature varying viscosity and showed that the steady migration velocity is a linear combination of the velocity for purely thermocapillary motion and the buoyancy-driven rising velocity. However, later, Zhang *et al.*[16] found that inclusion of inertia is crucial in the development of an asymptotic solution for small Marangoni numbers in the presence of temperature field. These studies, although took the viscosity stratification due to temperature gradient into account, the influence of viscosity stratification alone was not provided.

Viscosity stratifications achieved due to the presence of temperature and concentration gradients are continuous. Gradual viscosity variations can be naturally found in the mantle liquid below earth's crust and oceans. The stratification can also be achieved without the presence of temperature and concentration gradients. In several applications,[17] immiscible fluid-layers of almost the same density, but significant viscosity jump are observed. Bubble rise through an interface of two immiscible liquids of different viscosities has been studied in the past by several researchers.[18–20] Practically, all phenomena concerning viscosity stratification invariably include density gradient and other factors, which also influence the dynamics. Although, viscosity stratification is expected to play a significant role, with all the factors included, it is impossible to isolate the effect of viscosity stratification from the dynamics of rising bubble. Therefore, the objective of the present study is to separate the other effects and study the significance of the viscosity stratification alone for different regimes of bubble motion under the action of gravity. For the sake of completeness, below we discuss briefly the bubble rise dynamics inside a fluid of uniform viscosity and density; however, we restrict ourselves to single bubble/drop only.

A vast number of theoretical, numerical, and experimental work have been conducted[21–32] on single bubble rising in quiescent liquid of uniform density and viscosity. They investigated the terminal velocity, the deformation, and the path instability as the bubble translates in the upward direction. In a recent work, Tripathi *et al.*[33] studied the dynamics of an initially spherical bubble rising in quiescent liquid and identified regimes of starkly distinct behaviours in the Galilei (Ga) and Eötvös (Eo) numbers plane. It has been observed that increasing the Galilei number results in asymmetry in the path of the bubble, and a further increase in Ga results in breakup for the values of Eo beyond a certain limit. It is also well known that a bubble rising in a straight line may attain a variety of shapes which could be classified into spherical, ellipsoidal, dimpled ellipsoidal, skirted, and spherical cap shapes. For small values of Ga and Eo, bubble shapes in these regimes can be obtained by axisymmetric formulation.[33] In the present study, we restrict our analysis to the

axisymmetric regime only. In another recent work, Tripathi *et al.*[34] theoretically investigated the similarities and differences of the bubble and drop in axisymmetric regime. They found that bubble can be made to behave similar to a drop only for density ratios close to one and for low *Ga* and *Eo*. In general, the dynamics of bubble and drop are very different as the vortical regions prefer to be situated inside the lighter fluid, i.e., inside for bubbles and outside for drops.

Numerical simulations of such flows are very challenging due to the presence of interfacial dynamics and complexity of surface deformation. These problems are also computationally time consuming and very demanding. Thus, many researchers[24–26,28,29,35] have developed efficient computational techniques to solve these complicated dynamics. Several numerical methods have been proposed in the literature, ranging from boundary-fitted grids[36,37] to the level-set method,[38,39] the volume of fluid (VOF) method,[40] diffuse-interface methods,[41] and hybrid schemes of the Lattice-Boltzmann and the finite difference method.[42] Also, Bonometti and Magnaudet[43] developed a numerical technique which combines volume of fluid and level-set methods.

In the present study, the dynamics of rising gas bubble under the action of buoyancy inside an unbounded domain consisting of another fluid, whose viscosity increases linearly in the vertical direction, as shown in Fig. 1, is considered. An open-source fluid flow solver, Gerris, created by Popinet[44] is used, wherein a VOF method based on height-functions using balanced-force formulation has been implemented. Grid has been refined using an adaptive grid refinement technique in the interfacial and strong vortical regions. Our results for high values of *Ga* and *Eo* demonstrate a counter-intuitive phenomenon that the bubble undergoes extensive deformation by forming elongated skirt for linearly increasing viscosity medium. This is due to the translation of less viscous fluid, which is trapped inside the wake region bounded by the skirt of the bubble. This dynamics is very different from that observed in constant viscosity medium. For lower values of *Eo* and *Ga*, although the bubble moves slowly in case of the linearly increasing viscosity medium, the shapes look very similar for those observed in constant viscosity medium.

The rest of the paper is organized as follows. In Section II, we outline the formulation and governing equations, and in Section III, we discuss the numerical method used and present the validation by comparing the results obtained using the present solver with those reported in the

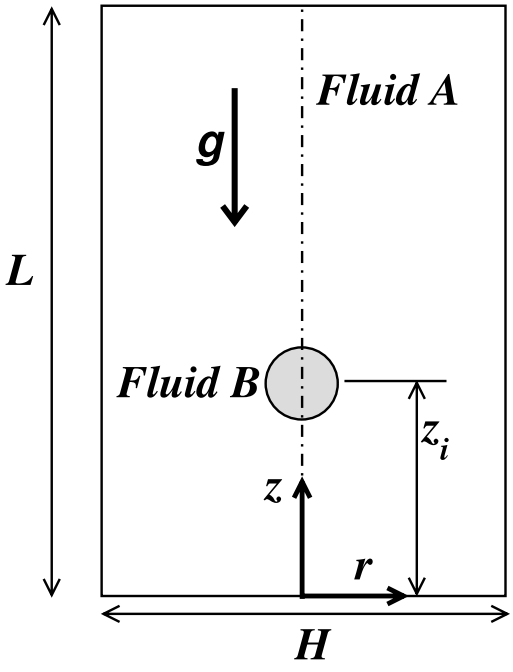

FIG. 1. Schematic diagram showing the initial configuration of a bubble (fluid "*B*") rising inside a viscosity stratified medium (fluid "*A*") under the action of gravity, which is acting in the negative z direction. Initially, the bubble is located at $z = z_i = 4R$, R being the radius of the bubble. The viscosity of the surrounding fluid "*A*" is linearly increasing along the vertical direction, z.

previous experimental and numerical studies. We then discuss our results in Section IV. Finally, concluding remarks are given in Section V.

II. FORMULATION

We numerically investigate the dynamics of an axisymmetric air bubble (designated by fluid "B") of initial radius R, having constant viscosity μ_B rising under the action of buoyancy inside an unbounded domain consisting of another fluid (designated by fluid "A"), as shown in Fig. 1, using VOF approach. Both the fluids are considered to be incompressible and Newtonian. The viscosity and density of fluids "A" and "B" are μ_A, ρ_A and μ_B, ρ_B, respectively. We use cylindrical coordinates (r, z) to model the rising bubble dynamics starting from a position $z_i = 4R$ at time $t = 0$ in quiescent liquid. Here, r and z are the radial and vertical coordinates, respectively. The viscosity field of fluid "A," μ_A, is initialized as $\mu_A = \mu_0(a_1 + a_2 z)$, μ_0 being the viscosity of fluid "A" at $z = z_i$, and a_1 and a_2 are constants, which are defined below. The flow dynamics is assumed to be symmetrical about $r = 0$, and the acceleration due to gravity, g, is acting in the negative z direction, as shown in Fig. 1. The governing equations of the problem are

$$\nabla \cdot \mathbf{u} = 0, \tag{1}$$

$$\rho\left[\frac{\partial \mathbf{u}}{\partial t} + \mathbf{u}\cdot\nabla\mathbf{u}\right] = -\nabla p + \nabla\cdot\left[\mu(\nabla\mathbf{u} + \nabla\mathbf{u}^T)\right] + \delta\sigma\kappa\mathbf{n} - \rho g\vec{e}_z, \tag{2}$$

$$\frac{\partial c}{\partial t} + \mathbf{u}\cdot\nabla c = 0, \tag{3}$$

$$\frac{\partial \mu}{\partial t} + \mathbf{u}\cdot\nabla\mu = 0, \tag{4}$$

where $\mathbf{u}(u, v)$ represents axisymmetric velocity field, wherein u and v are the velocity components in the radial and vertical directions, respectively; p denotes the pressure field; c is the volume fraction of the fluid "A," whose values are 0 and 1 for the air and liquid phases, respectively; μ is the viscosity field which is advected with the local velocity of the fluid; δ is the Dirac delta function; $\kappa = \nabla\cdot\mathbf{n}$ is the curvature, $\mathbf{n}$ is the unit normal to the interface pointing towards fluid "A," $\vec{e}_z$ represents the unit vector in the vertically upward direction, and σ is the interfacial tension coefficient of the liquid-gas interface.

The density, ρ, is calculated as a volume averaged quantity as follows:

$$\rho = \rho_B(1 - c) + \rho_A c. \tag{5}$$

The following scaling is employed in order to render the governing equations dimensionless,

$$(r, z) = R\,(\widetilde{r}, \widetilde{z})\,,\ t = \frac{R}{V}\widetilde{t},\ (u, v) = V(\widetilde{u}, \widetilde{v}),\ p = \rho_B V^2\widetilde{p},\ \mu = \widetilde{\mu}\mu_0,\ \rho = \widetilde{\rho}\rho_B, \tag{6}$$

where $V = \sqrt{gR}$ is the velocity scale, and the tildes designate dimensionless quantities. After dropping tildes from all nondimensional terms, the governing dimensionless equations are given by

$$\nabla \cdot \mathbf{u} = 0, \tag{7}$$

$$\rho\left[\frac{\partial \mathbf{u}}{\partial t} + \mathbf{u}\cdot\nabla\mathbf{u}\right] = -\nabla p + \frac{1}{Ga}\nabla\cdot\left[\mu(\nabla\mathbf{u} + \nabla\mathbf{u}^T)\right] + \frac{\delta}{Eo}\hat{n}\nabla\cdot\hat{n} - \rho\vec{e}_z, \tag{8}$$

$$\frac{\partial c}{\partial t} + \mathbf{u}\cdot\nabla c = 0, \tag{9}$$

$$\frac{\partial \mu}{\partial t} + \mathbf{u}\cdot\nabla\mu = 0, \tag{10}$$

where $Ga(\equiv \rho_B V R/\mu_B)$ and $Eo(\equiv \rho_B g R^2/\sigma)$ denote the Galilei number and Eötvös number, respectively. The dimensionless density ρ is given by

$$\rho = (1 - c) + \rho_r c, \tag{11}$$

and the initial viscosity field is given by:

$$\mu = (1 - c) + \mu_{r0}(a_1 + a_2 z)c, \tag{12}$$

where $\mu_{r0} \equiv \mu_0/\mu_B$ and $\rho_r \equiv \rho_A/\rho_B$. Note that by setting $a_1 = 1$ and $a_2 = 0$, one could recover a system with constant viscosity of the surrounding fluid.

III. NUMERICAL METHOD

In the present study, a finite-volume open source code, *Gerris*,[34,44] is used to solve Eqs. (7)-(9). The interface between the two fluids is captured using the VOF approach with dynamic adaptive grid refinement based on the vorticity magnitude and position of the interface. This solver also minimizes the spurious currents (to the machine error) at the interface (which are known to appear when the density ratio and the interfacial tension are high) by incorporating a balanced force height-function continuum-surface-force formulation[46,47] for the inclusion of the surface force term in the Navier-Stokes equations. The flow is assumed to be symmetrical about the axis $r = 0$, and the Neumann boundary conditions are imposed at the rest of the boundaries of the computational domain. We refer the readers to the work of Tripathi *et al.*[13,34] for detailed description of the numerical method used in this study.

A. Validations

The present solver has been validated extensively by comparing the results obtained from the present simulations with the previously reported numerical and experimental results. The evolution of shapes of the bubble at different times for $Ga = 10$, $Eo = 0.2$, $\rho_r = 10^3$, and $\mu_r = 10^2$ are presented in Fig. 2. It can be seen that for this set of parameters, the bubble is almost spherical till $t = 0.4$. For $t > 0.4$, the bubble undergoes significant deformation and subsequent topological change at $t = 1.6$. Thereafter, the bubble continues to move in the upward direction as an annular doughnut-like structure. It is to be noted here that the bubble shapes presented in Fig. 2 are in excellent agreement with the numerical simulation (level-set method) results of Sussman and Smereka[45] for this set of parameters.

Next, we have validated our numerical method by comparing the terminal shapes and streamlines with the experimental results of Bhaga and Weber[31] for different values of Ga and Eo in Figs. 3 and 4, respectively. In Fig. 3, the pictures in the black and white background are the experimental results of Bhaga and Weber[31] and the red lines show the terminal shape of the bubble obtained from

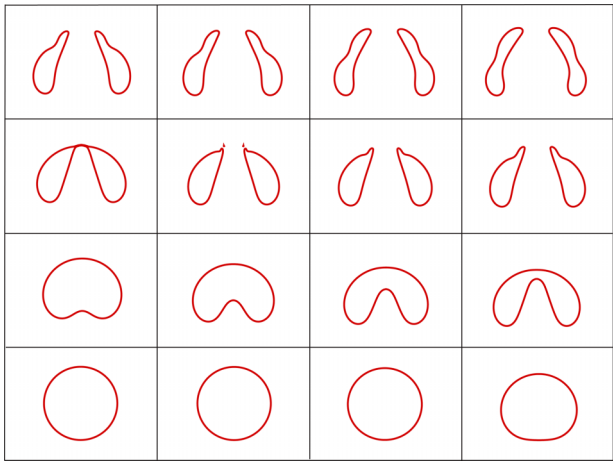

FIG. 2. The time evolution of the shapes of the bubble for the constant viscosity case ($a_1 = 1$, $a_2 = 0$) for $Ga = 10$, $Eo = 0.2$, $\rho_r = 10^3$, and $\mu_{r0} = 10^2$. From left to right and from bottom to top, $t = 0$, 0.2, 0.4, 0.6, 0.8, 1, 1.2, 1.4, 1.6, 1.8, 2, 2.2, 2.4, 2.6, 2.8, and 3. The shapes of the bubble agree well with those presented in the work of Sussman and Smereka.[45]

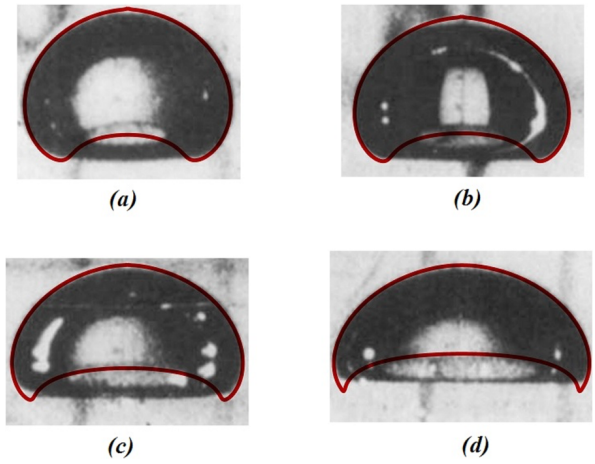

FIG. 3. Comparison of the terminal shapes of the bubble obtained from the present simulations (shown by red lines) with those presented in the work of Bhaga and Weber[31] (background picture) for different values of Ga: (a) $Ga = 0.167$, (b) $Ga = 0.222$, (c) $Ga = 0.355$, and (d) $Ga = 0.586$. The rest of the parameter values are $Eo = 0.021$, $\rho_r = 1.39 \times 10^3$, and $\mu_{r0} = 10^2$.

the present simulations. In Fig. 4, the left and right hand sides in each panel represent the present simulation results and the experimental results, respectively. It can be seen that the bubble shapes and the streamline patterns are in excellent agreement. We have also performed several other validation exercises by comparing our results with previous experimental[48] and computational[32] works (see the supplementary material of Refs. 13, 33, and 34). Our grid convergence test (not shown) reveals that grid convergence is achieved for simulations with the smallest grid size less than 0.016. Thus, all the results presented in the paper are obtained using this grid in a computational domain of size 16×48. Also, it has been ensured that further increase in the size of the computational domain has negligible effect on the bubble dynamics. For the rest of the investigation, the density and initial viscosity ratios are considered to be $\rho_r = 10^3$ and $\mu_{r0} = 10^2$, respectively.

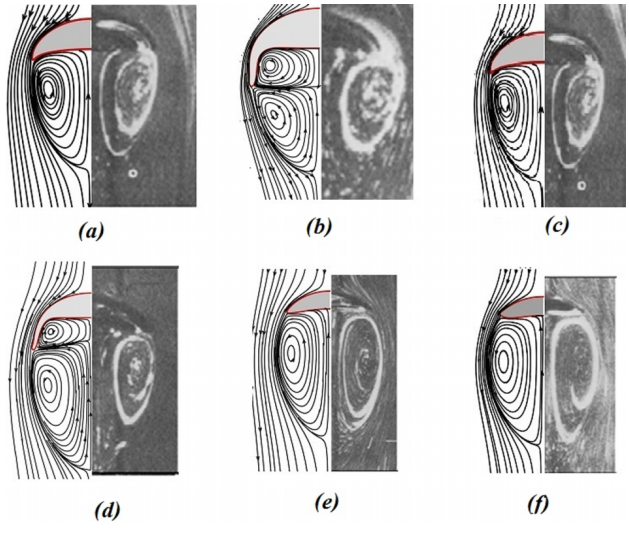

FIG. 4. Comparison of streamline patterns along with the terminal shapes of the bubble (shown by red lines) obtained from the present simulation (on the left hand side of each panel) with those presented in the work of Bhaga and Weber[31] (right hand side of each panel) for (a) $Ga = 0.79$, $Eo = 0.017$; (b) $Ga = 0.9$, $Eo = 0.021$; (c) $Ga = 1.26$, $Eo = 0.017$; (d) $Ga = 1.78$, $Eo = 0.027$; (e) $Ga = 2.19$, $Eo = 0.017$; and (f) $Ga = 3.32$, $Eo = 0.011$. The rest of the parameter values are $\rho_r = 1.39 \times 10^3$ and $\mu_{r0} = 10^2$.

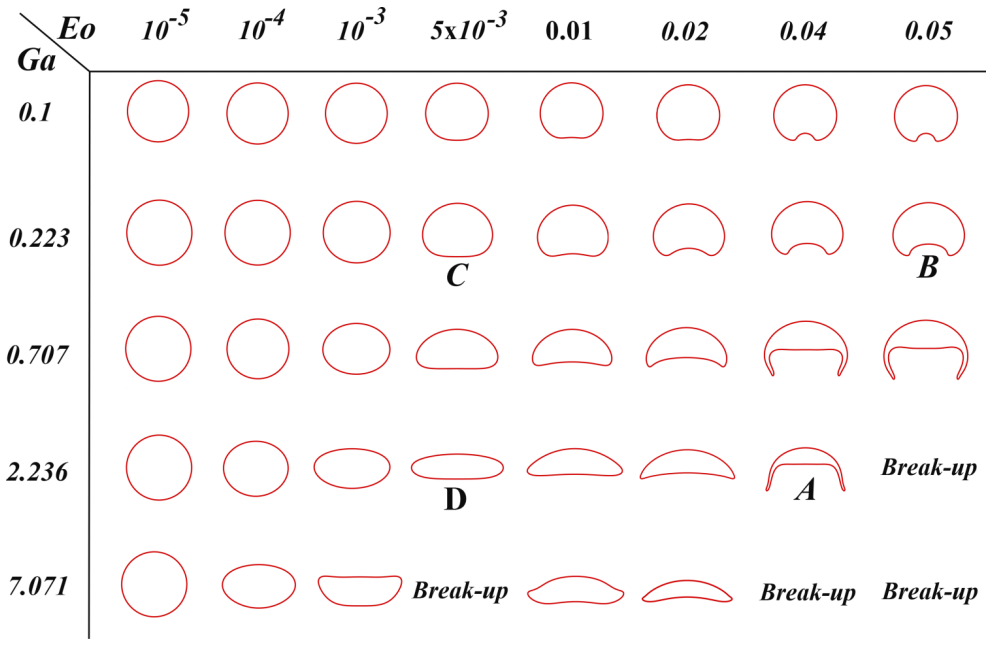

FIG. 5. The terminal shapes of the bubble obtained from the present simulations in $Ga-Eo$ space for the constant viscosity case ($a_1 = 1, a_2 = 0$). The rest of the parameter values are $\rho_r = 10^3$ and $\mu_{r0} = 10^2$.

IV. RESULTS AND DISCUSSION

We begin the presentation of our results in Fig. 5 by plotting the terminal shapes of the bubble for the constant viscosity case ($a_1 = 1, a_2 = 0$) obtained from our time-dependent simulations in $Ga - Eo$ space. Below, this is referred to as the "base case." A similar plot based on the steady state calculations was presented by Tsamopoulos *et al.*[49] Note that in their study, the viscosity and density of the surrounding fluid were used as the characteristic scales to nondimensionalize the governing equations; hence, a suitable conversion is applied to get our dimensionless variables. We found that for low Ga and low Eo, the shapes of the bubble presented in Fig. 5 are qualitatively similar to those obtained by Tsamopoulos *et al.*[49] However, the shapes of the bubble are different for larger values of Eo and Ga. This discrepancy can be attributed to the steady state assumption considered in their study. We also found that the bubble undergoes topological changes and the bubble dynamics remain unsteady for few sets of Ga and Eo (designated by "breakup" in Fig. 5). The time evolution of shapes of the bubble for one typical "breakup" case ($Ga = 7.071$ and $Eo = 0.05$) is shown in Fig. 6. It can be seen in this figure that bubble has a different topology for $t > 2$ for this set of parameters. Note that Tsamopoulos *et al.*[49] also did not find a steady state solution for cases designated by "breakup."

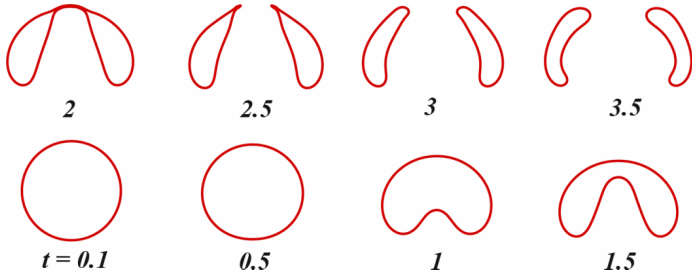

FIG. 6. Time evolution of the shapes of the bubble obtained for a typical "breakup" case ($Ga = 7.071$ and $Eo = 0.05$). The rest of the parameter values are the same as those used to generate Fig. 5. The dimensionless time is written at the bottom of each bubble.

The effect of viscosity stratification of the surrounding fluid (for a system where the viscosity increases with increasing z) on the bubble dynamics is investigated next. The viscosity of the surrounding fluid (at rest, $t = 0$) is given by

$$\mu_A = \mu_{r0}(a_1 + a_2 z), \tag{13}$$

where values of the constants a_1 and a_2 are fixed at 0.2.

The bubble rise dynamics of four typical sets of (Ga, Eo) designated by points A, B, C, and D in Fig. 5, which correspond to $(Ga, Eo) = (2.236, 0.04), (0.223, 0.05), (0.223, 0.005)$, and $(2.236, 0.05)$, respectively, are investigated below. The behaviour of the rest of the bubbles in Fig. 5 can be extrapolated from these four typical cases analyzed below.

A. Point A: *Ga* = 2.236, *Eo* = 0.04

The temporal evaluation of bubble shapes for $Ga = 2.236, Eo = 0.04$ is shown in Fig. 7. The shapes of the bubble in linearly increasing viscosity medium (shown in Fig. 7(b)) are compared with those of constant viscosity case (shown in Fig. 7(a)) at different times. It can be seen that for the case of the linearly increasing viscosity medium, an elongated skirt (longer than that appears for the constant viscosity case (Fig. 7(a))) is formed leading to a single recirculation region (as shown in Fig. 8(b)). This is counter-intuitive due to the fact that as the bubble rises in the vertical direction, the local viscosity increases, which in turn decreases the local Ga. It has been observed that at lower Ga, the bubble tends to take a dimpled ellipsoidal shape instead of forming skirt (see, for instance, the bubble shapes for $Eo = 0.04$ in Fig. 5). As the bubble rises in the upward direction, the less viscosity fluid from the bottom part of the domain advects along with the recirculation region. Thus,

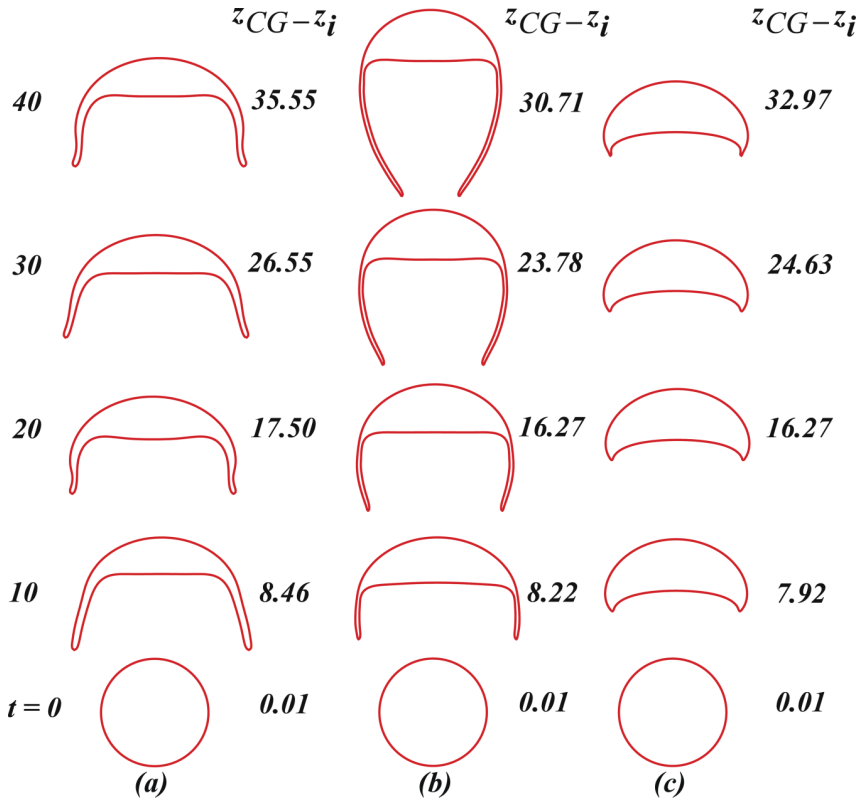

FIG. 7. Time evolution of bubble shapes for $Ga = 2.236, Eo = 0.04$: (a) constant viscosity system ($a_1 = 1, a_2 = 0$), (b) linearly increasing viscosity ($a_1 = 0.2, a_2 = 0.2$), (c) constant viscosity case in which μ_{r0} is set to the average viscosity of the linearly increasing viscosity system (panel (b)) for the distance traversed by the center of gravity of the bubble (μ_{avg}).

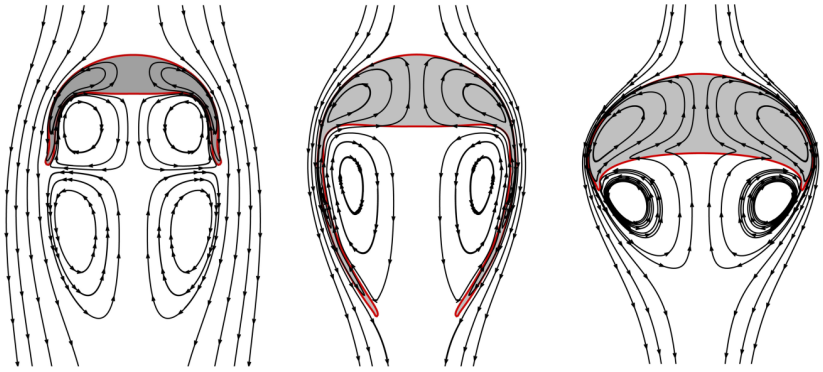

FIG. 8. Comparison of the streamlines at $t = 40$ for (a) constant viscosity system ($a_1 = 1, a_2 = 0$), (b) linearly increasing viscosity ($a_1 = 0.2, a_2 = 0.2$), (c) constant viscosity case in which μ_{r0} is set to the average viscosity of the linearly increasing viscosity system (panel (b)) for the distance traversed by the center of gravity of the bubble (μ_{avg}). The rest of the parameter values are the same as those used to generate Fig. 7.

the viscosity contrast between inside and outside regions separated by the skirt continues to increase with the ascent of the bubble. The stresses generated due to the differential viscosity on both sides of the skirt force it to curl inwards. This deformation of the skirt leads to a physical separation of the two regions with high viscosity contrast by means of the air film contained in the skirt of the bubble. This separation of fluids allows fast recirculation to occur in the fluid captured inside the wake of the bubble, while simultaneously allowing a slow flow outside of the skirt, thus creating a contrast in Reynolds number as well. This may be beneficial to certain processes where a low viscosity fluid is required to be carried through a highly viscous fluid with the help of a carrier bubble.

In order to investigate whether this dynamics is due to our viscosity scale, we re-examine how the results reflect our choice of viscosity scale. In Fig. 7(c), the evolution of shapes of the bubble is plotted for constant outer fluid viscosity equal to the average of the lowest (i.e., μ_A at $z = 0$) and highest (i.e., μ_A at $z = 30.71$) viscosity values, i.e., the average viscosity of the linearly increasing viscosity system (Fig. 7(b)) for the distance traversed by the center of gravity of the bubble (μ_{avg}). As there is no ideal viscosity scale, we have made this simplest choice possible. It can be seen in Fig. 7(c) that the skirt formation delays significantly (starts at $t \approx 32$) as compared to the cases presented in Figs. 7(a) and 7(b). It is surprising that the bubble rise velocity in Fig. 7(c) is almost the same as those of the cases presented in Figs. 7(a) and 7(b), suggesting that the wake viscosity plays an important role in skirt formation and the deformation of the bubble. The viscosity distribution for the linearly increasing viscosity case at later time, $t = 40$ (shown in Fig. 9), reveals that as

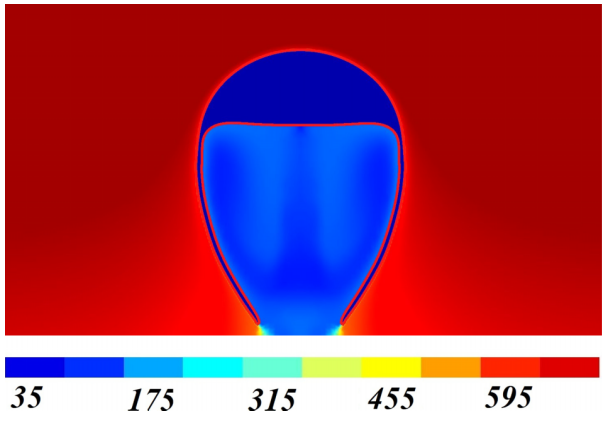

FIG. 9. Viscosity contours for the linearly increasing viscosity case at $t = 40$. The rest of the parameter values are the same as those used to generate Fig. 7(b).

the bubble rises, it carries the low viscosity fluid from the bottom part of the domain in its wake region. Thus, it can be deduced from Figs. 7(a) and 7(b) that the stresses inside the wake affect the formation of skirt the most, which can be expressed as the local *Ga* and *Eo* inside the skirt. This is confirmed by the fact that Fig. 7(c) forms skirt at later times since the local *Ga* in the wake is not favourable (lesser than the corresponding value of *Ga* in Figs. 7(a) and 7(b)) to form skirt.

In Fig. 8, the streamlines in the reference frame moving with the same velocity as that of the tip of the bubble at $t = 40$ are plotted for the same parameter values as those used to generate Fig. 7. It is also noted here that the wake structures of the constant viscosity and linearly increasing viscosity cases are very different from each other, as shown in Fig. 8. For the constant viscosity system ($a_1 = 1, a_2 = 0$) with $\mu_{r0} = 100$ (Fig. 8(a)), it can be seen that there are two recirculation zones in the wake region of the bubble, whereas the bubble in linearly increasing viscosity medium (Fig. 8(b)) shows only one recirculation zone in its wake region which is enclosed by the skirt. The two recirculation zones in the wake of the bubble corresponding to Fig. 8(a) prevent the skirt from closing in on itself, and depending on the strength of circulation in the two zones, the skirt may develop travelling waves on the skirt which is termed as wavy skirt.[31] Close inspection of Fig. 8(c) reveals that the streamlines cross the air-liquid interface in the wake region, which implies that the shape is far from steady and the skirt may become longer at later times. It can also be inferred from the streamline patterns of Fig. 8(c) that there must be two toroidal recirculation zones inside the bubble of which only one can be seen by choosing the frame of reference moving with the tip of the bubble. There must be a counter-rotating vortex inside the bubble in order to satisfy the continuity of stress and velocity components inside the bubble between the two co-rotating vortices which are shown in this figure. Inspection of contours of vorticity magnitude plotted in Fig. 10 reveals that the maximum vorticity always lies inside the bubble. A similar finding was also observed by Tripathi *et al.*[34]

The temporal variations of rise velocity (v_z) and aspect ratio ($a_r = h/w$) of the bubble for all the cases considered in Fig. 7 are shown in Figs. 11(a) and 11(b), respectively. Fig. 11(a) shows an expected behaviour; the bubbles for constant viscosity cases attain a terminal velocity. However, the bubble in linearly increasing viscosity medium (shown in Fig. 7(b)) keeps decelerating, with a peak at an early time (approximately at $t = 2$). The peak may be attributed to the initial acceleration due to buoyancy, and the gradual decay in the rise velocity is due to the viscous forces overcoming the gravitational forces at later times. This is evident from the ratio of the viscous and the gravitational time scales ($\sqrt{R/g}/(\rho R^2/\mu)$), which is the Galilei number. It can be seen in Fig. 11(a) that the viscous force overcomes the gravitational force (when the rise velocity reaches a maximum) at $t \approx 2$ which approximately matches with the value of Galilei number considered. In Fig. 11(b), it can be seen that the bubble reaches to a terminal oblate shape for constant viscosity cases. The aspect ratio of the bubble, when the outer fluid viscosity is $\mu_{r0} = \mu_{avg}$, is higher than that when $\mu_{r0} = 100$ (base case). In case of linearly increasing viscosity system, the bubble becomes oblate by decreasing the value of a_r to approximately 0.2, which subsequently increases gradually with time.

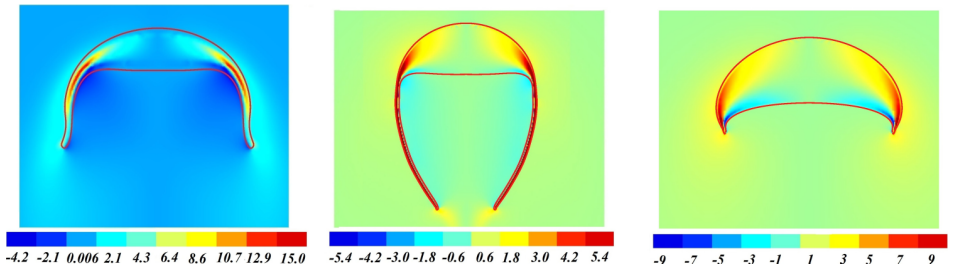

(a) (b) (c)

FIG. 10. Vorticity magnitude at $t = 40$ for (a) constant viscosity system ($a_1 = 1, a_2 = 0$), (b) linearly increasing viscosity case ($a_1 = 0.2, a_2 = 0.2$), (c) constant viscosity case in which μ_{r0} is set to the average viscosity of the linearly increasing viscosity system (panel (b)) for the distance traversed by the center of gravity of the bubble (μ_{avg}). The rest of the parameter values are the same as those used to generate Fig. 7.

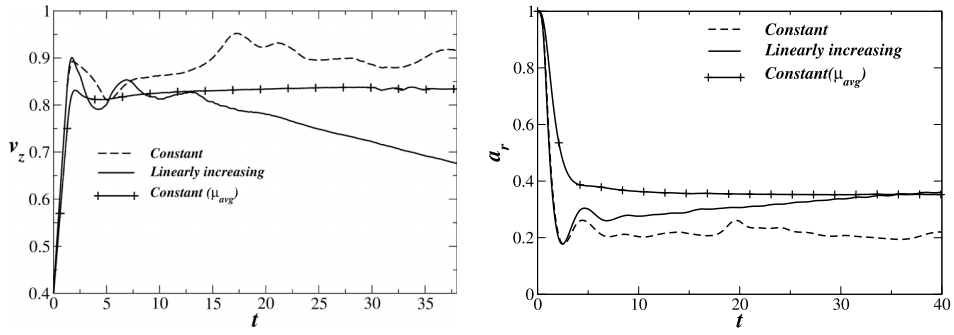

(a) (b)

FIG. 11. Variation of the (a) rise velocity (v_z) and (b) aspect ratio ($a_r = h/w$) of the bubble with time. Here, h and w represent the height and width of the bubble. The rest of the parameter values are the same as those used to generate Fig. 7.

B. Point B: *Ga* = 0.223, *Eo* = 0.05

Next, in Fig. 12, we investigate the dynamics associated with the bubble marked as point "B" in Fig. 5 ($Ga = 0.223, Eo = 0.05$). In this case, Eo is slightly higher, but Ga is ten times lower than the value used for the bubble designated by point "A" (discussed above). It can be seen in Fig. 12 that the shapes of the bubble at different times for linearly increasing viscosity medium (Fig. 12(b)) and constant viscosity system ($a_1 = 1, a_2 = 0$) (Fig. 12(a)) are similar. However, these are qualitatively different from the shapes exhibited by bubble shown in Fig. 12(c). This result also suggests that the bubble dynamics is predominantly dominated by the wake region of the bubble. Inspection of this figure also reveals that the cross section of the bubbles in panels (a) and (b) is elliptical, but in panel

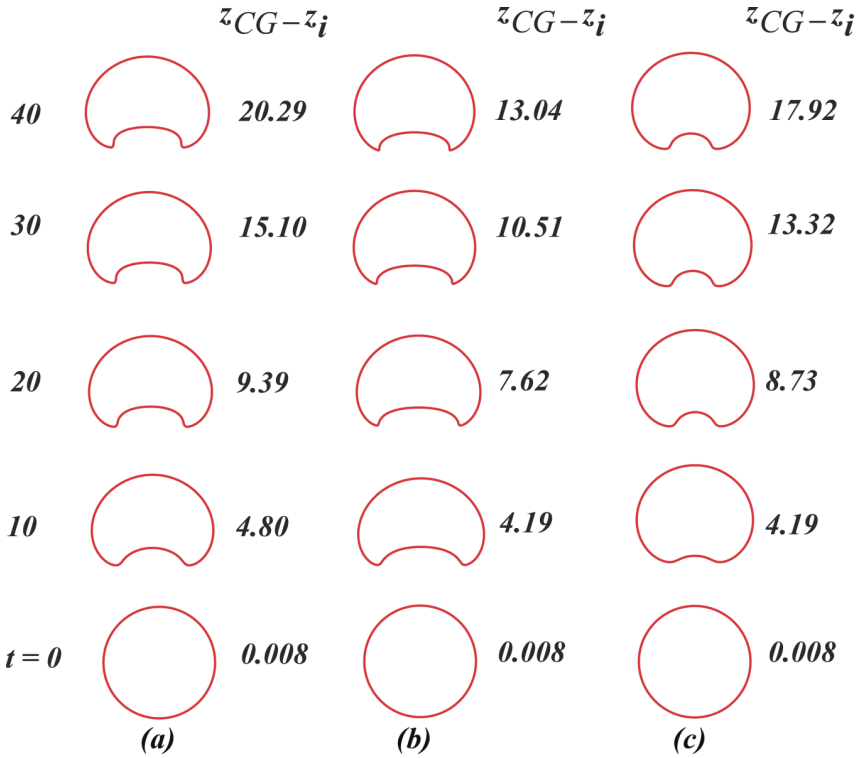

FIG. 12. Time evolution of bubble shapes for $Ga = 0.223, Eo = 0.05$: (a) constant viscosity system (base case) ($a_1 = 1, a_2 = 0$), (b) linearly increasing viscosity case ($a_1 = 0.2, a_2 = 0.2$), (c) constant viscosity case in which μ_{r0} is set to the average viscosity of the linearly increasing viscosity system (panel (b)) for the distance traversed by the center of gravity of the bubble (μ_{avg}).

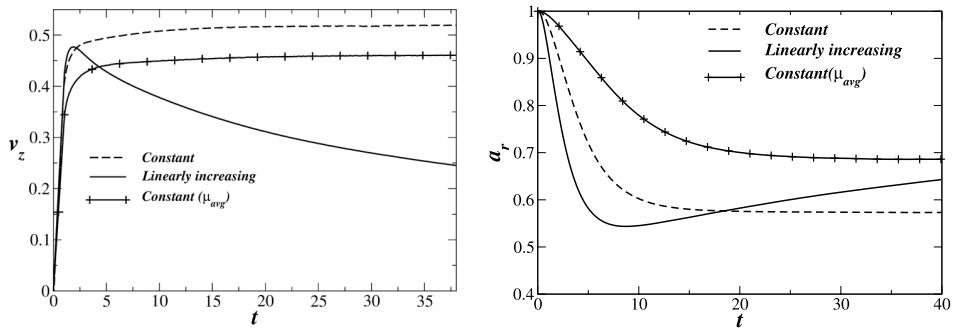

(a) (b)

FIG. 13. Variation of velocity of the center of gravity and aspect ratio of the bubble with time. The rest of the parameter values are the same as those used to generate Fig. 12.

(c), it is more or less semicircular. The variation of center of gravity and aspect ratio of the bubbles presented in Fig. 12 are shown in Figs. 13(a) and 13(b), respectively. It can be seen that the bubbles for constant viscosity cases (Figs. 12(a) and 12(c)) attain terminal shape and velocity. However, the bubble in linearly increasing viscosity medium (shown in Fig. 12(b)) decelerates, with a peak at an early time. The early accelerating phase is driven by the initial acceleration due to buoyancy. In Fig. 13(b), it can be seen that the aspect ratio of the bubble inside a linearly increasing viscosity medium decreases (approximately to $a_r = 0.55$) and it assumes an oblate shape, after which the bubble has a tendency to go towards the original shape. It is to be noted that the bubble for this case has not reached a steady state and expected to deform continuously with time.

C. Point C: *Ga* = 0.223, *Eo* = 5 × 10^{-3}

In Fig. 14, the shapes of the bubble for $Ga = 0.223, Eo = 5 \times 10^{-3}$ are plotted. It is to be noted here that both *Ga* and *Eo* are small. In this case, the surface tension dominates the dynamics; the

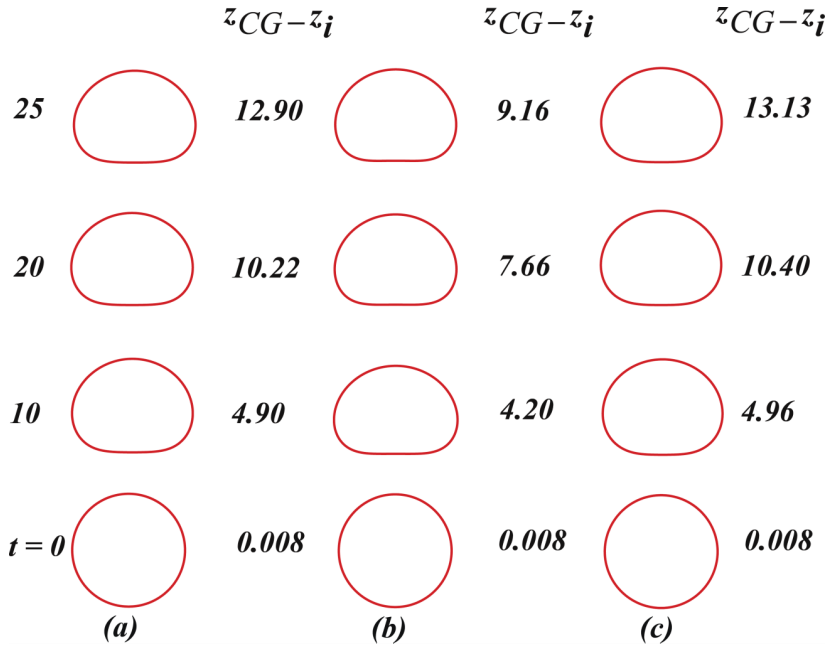

FIG. 14. Time evolution of bubble shapes for $Ga = 0.223, Eo = 0.005$: (a) constant viscosity system ($a_1 = 1, a_2 = 0$), (b) linearly increasing viscosity case ($a_1 = 0.2, a_2 = 0.2$), (c) constant viscosity case in which μ_{r0} is set to the average viscosity of the linearly increasing viscosity system (panel (b)) for the distance traversed by the center of gravity of the bubble (μ_{avg}).

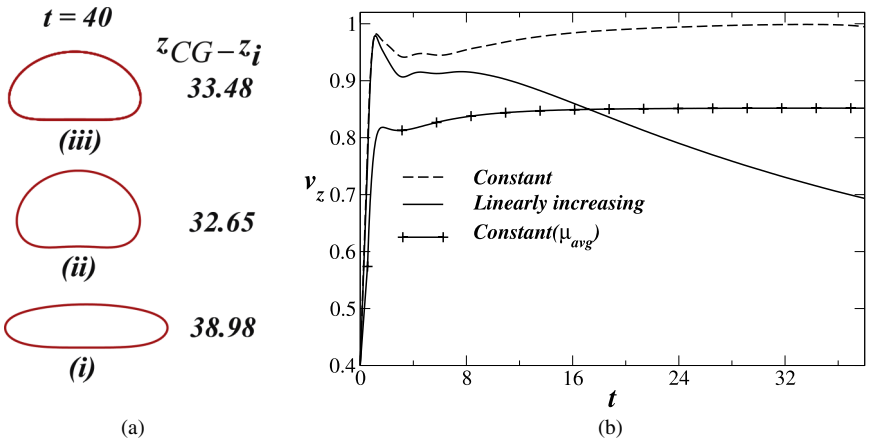

FIG. 15. (a) Terminal shape of the bubbles: (i) constant viscosity system ($a_1 = 1, a_2 = 0$), (ii) linearly increasing viscosity case ($a_1 = 0.2, a_2 = 0.2$), (iii) constant viscosity case in which μ_{r0} is set to the average viscosity of the linearly increasing viscosity system (panel (ii)) for the distance traversed by the center of gravity of the bubble (μ_{avg}). (b) Variation of velocity of the center of gravity of the bubble with time. The rest of the parameter values are $Ga = 2.236$ and $Eo = 5 \times 10^{-3}$.

shapes of the bubble become slightly oblate after reaching an apparent steady state at very early time (for $t > 10$). However, it can be seen that as the *Ga* considered in this case is very low, the velocity of the bubbles for constant viscosity cases (panels (a) and (c)) is nearly the same. However, in case of linearly increasing viscosity medium (panel (b)), the velocity of the bubble decreases as the local *Ga* decreases further due to the increase in local viscosity as the bubble moves in the upward direction.

D. Point D: *Ga* = 2.236, *Eo* = 5 × 10^{-3}

The terminal shapes of the bubbles for $Ga = 2.236, Eo = 5 \times 10^{-3}$ corresponding to the case "D" in Fig. 5 are shown in Fig. 15(a). It can be seen that the shapes of the bubbles for the linearly increasing viscosity medium (shown in sub-panel (ii) of Fig. 15(a)) and constant viscosity case when μ_{r0} is set to μ_{avg} (sub-panel (iii) of Fig. 15(a)) are almost similar (oblate shape). However, the dimple of the bubble in case of the linearly increasing viscosity medium (sub-panel (ii) of Fig. 15(a)) is not visible in sub-panel (iii) of the same figure. It can also be seen in sub-panel (i) that the bubble takes a disk like shape for the base case ($a_1 = 1, a_2 = 0$). The velocity of the centre of gravity versus time plot (Fig. 15(b)) confirms the above-mentioned conclusion. Inspection of this figure also reveals that the bubble in linearly increasing viscosity medium decelerates after the accelerating phase is observed during the early time.

V. CONCLUDING REMARKS

In this paper, we have examined the axisymmetric dynamics of bubble rise in an unconfined viscosity stratified medium. An open-source finite-volume flow solver, *Gerris*, based on volume-of-fluid methodology is used to investigate the flow, which involves the numerical solution of the equations of mass and momentum conservation and an equation of the volume fraction of the surrounding fluid. In spite of the large number of studies carried out on bubbles and drops, very few studies have examined the influence of viscosity stratification (to the best of our knowledge, none of them isolate the effects of viscosity-stratification) on the bubble rise dynamics. We have presented a library of bubble shapes in the Galilei and the Eötvös numbers plane. The present results (terminal shapes of the bubbles) agree well with those obtained by Tsamopoulos *et al.*[49] for low *Ga* and low *Eo*. The shapes of the bubbles are qualitatively different for higher values of *Ga* and *Eo*. This difference may be attributed to the steady state calculations conducted in their study. Our results demonstrate a counter-intuitive phenomenon that the bubble undergoes extensive deformation

by forming elongated skirt for linearly increasing viscosity medium for certain sets of parameter values. This is due to the migration of less viscous fluid, which is trapped inside the wake region bounded by the skirt of the bubble. This dynamics is very different from that observed in constant viscosity medium. We found that for lower values of *Eo* and *Ga*, although the bubble moves slowly in case of the linearly increasing viscosity medium, the shapes look very similar to those observed in constant viscosity medium. In future, it will be interesting to investigate this phenomenon in three-dimensions and by conducting experiments.

ACKNOWLEDGMENTS

We would like to thank the Indian National Science Academy for their financial support.

[1] D. C. Blanchard, "Comments on the breakup of raindrops," J. Atmos. Sci. **19**, 119 (1962).
[2] B. Gal-Or, G. E. Klinzing, and L. L. Tavlarides, "Bubble and drop phenomena," Ind. Eng. Chem. **61**, 21 (1969).
[3] M. T. Ghannam and M. N. Esmail, "Rheological properties of carboxymethyl cellulose," J. Appl. Polym. Sci. **64**, 289 (1997).
[4] C. Beal *et al.*, "The viscosity of air, water, natural gas, crude oil and its associated gases at oil field temperatures and pressures," Trans. AIME **165**, 94 (1946).
[5] G. Urbain, Y. Bottinga, and P. Richet, "Viscosity of liquid silica, silicates and alumino-silicates," Geochim. Cosmochim. Acta **46**, 1061 (1982).
[6] N. O. Young, J. S. Goldstein, and M. J. Block, "The motion of bubbles in a vertical temperature gradient," J. Fluid Mech. **6**, 350 (1959).
[7] R. S. Subramanian, R. Balasubramaniam, and G. Wozniak, in *Physics of Fluids in Microgravity*, edited by R. Monti (Taylor and Francis, London, 2002), pp. 149–177.
[8] R. S. Subramanian, "Slow migration of a gas bubble in a thermal gradient," AIChE J. **27**, 646–654 (1981).
[9] R. S. Subramanian, "Thermocapillary migration of bubbles and droplets," Adv. Space Res. **3**, 145 (1983).
[10] R. Balasubramaniam and R. S. Subramaniam, "Thermocapillary bubble migration thermal boundary layers for large Marangoni numbers," Int. J. Multiphase Flow **22**, 593 (1996).
[11] R. Balasubramaniam and R. S. Subramanian, "The migration of a drop in a uniform temperature gradient at large Marangoni numbers," Phys. Fluids **12**, 733 (2000).
[12] A. Crespo, E. Migoya, and F. Manuel, "Thermocapillary migration of bubbles at large Reynolds numbers," Int. J. Multiphase Flow **24**, 685 (1998).
[13] M. K. Tripathi *et al.*, "Non-isothermal bubble rise: Non-monotonic dependence of surface tension on temperature," J. Fluid Mech. **763**, 82 (2015).
[14] R. M. Merritt, D. S. Morton, and R. S. Subramanian, "Flow structures in bubble migration under the combined action of buoyancy and thermocapillarity," J. Colloid Interface Sci. **155**, 200 (1993).
[15] R. Balasubramaniam, "Thermocapillary and buoyant bubble motion with variable viscosity," Int. J. Multiphase Flow **24**, 679 (1998).
[16] L. Zhang, R. S. Subramanian, and R. Balasubramaniam, "Motion of a drop in a vertical temperature gradient at small Marangoni number the critical role of inertia," J. Fluid Mech. **448**, 197 (2001).
[17] R. Govindarajan and K. C. Sahu, "Instabilities in viscosity-stratified flows," Annu. Rev. Fluid Mech. **46**, 331 (2014).
[18] M. Manga and H. A. Stone, "Low Reynolds number motion of bubbles, drops and rigid spheres through fluid–fluid interfaces," J. Fluid Mech. **287**, 279 (1995).
[19] R. Bonhomme, J. Magnaudet, F. Duval, and B. Piar, "Inertial dynamics of air bubbles crossing a horizontal fluid–fluid interface," J. Fluid Mech. **707**, 405 (2012).
[20] M. Kemiha *et al.*, "Passage of a gas bubble through a liquid-liquid interface," Ind. Eng. Chem. Res. **46**, 6099 (1991).
[21] S. Antal, R. Lahey, Jr., and J. Flaherty, "Analysis of phase distribution in fully developed laminar bubbly two-phase flow," Int. J. Multiphase Flow **17**, 635 (1991).
[22] B. Bunner and G. Tryggvason, "Direct numerical simulations of three-dimensional bubbly flows," Phys. Fluids **11**, 1967 (1999).
[23] J. Lu and G. Tryggvason, "Effect of bubble deformability in turbulent bubbly upflow in a vertical channel," Phys. Fluids **20**, 040701 (2008).
[24] M. Sussman and E. G. Puckett, "A coupled level set and volume-of-fluid method for computing 3D and axisymmetric incompressible two-phase flows," J. Comput. Phys. **162**, 301 (2000).
[25] S. Shin and D. Juric, "Modeling three-dimensional multiphase flow using a level contour reconstruction method for front tracking without connectivity," J. Comput. Phys. **180**, 427 (2002).
[26] J. Hua, J. F. Stene, and P. Lin, "Numerical simulation of 3D bubbles rising in viscous liquids using a front tracking method," J. Comput. Phys. **227**, 3358 (2008).
[27] W. Dijkhuizen, M. van Sint Annaland, and J. Kuipers, "Numerical and experimental investigation of the lift force on single bubbles," Chem. Eng. Sci. **65**, 1274 (2010).
[28] M. Pivello *et al.*, "A fully adaptive front tracking method for the simulation of two phase flows," Int. J. Multiphase Flow **58**, 72 (2014).
[29] M. Baltussen, J. Kuipers, and N. Deen, "A critical comparison of surface tension models for the volume of fluid method," Chem. Eng. Sci. **109**, 65 (2014).
[30] T. Taylor and A. Acrivos, "On the deformation and drag of a falling viscous drop at low Reynolds number," J. Fluid Mech. **18**, 466 (1964).

[31] D. Bhaga and M. E. Weber, "Bubbles in viscous liquids: Shapes, wakes and velocities," J. Fluid Mech. **105**, 61 (1981).
[32] J. Han and G. Tryggvason, "Secondary breakup of axisymmetric liquid drops. I. Acceleration by a constant body force," Phys. Fluids **11**, 3650 (1999).
[33] M. K. Tripathi, K. C. Sahu, and R. Govindarajan, "Dynamics of an initially spherical bubble rising in quiescent liquid," Nat. Commun. **6**, 6268 (2015).
[34] M. K. Tripathi, K. C. Sahu, and R. Govindarajan, "Why a falling drop does not in general behave like a rising bubble," Sci. Rep. **4**, 4771 (2014).
[35] W. Dijkhuizen, I. Roghair, M. Annaland, and J. Kuipers, "DNS of gas bubbles behaviour using an improved 3D front tracking model—Model development," Chem. Eng. Sci. **65**, 1427 (2010).
[36] J. C. Chen and Y. T. Lee, "Effect of surface deformation on thermocapillary bubble migration," AIAA J. **30**, 993 (1992).
[37] S. W. Welch, "Transient thermocapillary migration of deformable bubbles," J. Colloid Interface Sci. **208**, 500 (1998).
[38] H. Haj-Hariri, Q. Shi, and A. Borhan, "Thermocapillary motion of deformable drops at finite Reynolds and Marangoni numbers," Phys. Fluids **9**, 845 (1997).
[39] J.-F. Zhao, Z.-D. Li, H.-X. Li, and J. Li, "Thermocapillary migration of deformable bubbles at moderate to large Marangoni number in microgravity," Microgravity Sci. Technol. **22**, 295 (2010).
[40] C. Ma and D. Bothe, "Direct numerical simulation of thermocapillary flow based on the Volume of Fluid method," Int. J. Multiphase Flow **37**, 1045 (2011).
[41] R. Borcia and M. Bestehorn, "Phase-field simulations for drops and bubbles," Phys. Rev. E **75**, 056309 (2007).
[42] H. Liu, A. Valocchi, Y. Zhang, and Q. Kang, "Phase-field-based lattice Boltzmann finite-difference model for simulating thermocapillary flows," Phys. Rev. E **87**, 013010 (2013).
[43] T. Bonometti and J. Magnaudet, "An interface-capturing method for incompressible two-phase flows. Validation and application to bubble dynamics," Int. J. Multiphase Flow **33**, 109 (2007).
[44] S. Popinet, "Gerris: A tree-based adaptive solver for the incompressible Euler equations in complex geometries," J. Comput. Phys. **190**, 572 (2003).
[45] M. Sussman and P. Smereka, "Axisymmetric free boundary problems," J. Fluid Mech. **341**, 269 (1997).
[46] J. Brackbill, D. B. Kothe, and C. Zemach, "A continuum method for modeling surface tension," J. Comput. Phys. **100**, 335 (1992).
[47] S. Popinet, "An accurate adaptive solver for surface-tension-driven interfacial flows," J. Comput. Phys. **228**, 5838 (2009).
[48] R. Clift, J. Grace, and M. Weber, *Bubbles, Drops and Particles* (Academic, New York, 1978), p. 346.
[49] J. Tsamopoulos *et al.*, "Steady bubble rise and deformation in Newtonian and viscoplastic fluids and conditions for bubble entrapment," J. Fluid Mech. **601**, 123 (2008).